Physica Medica 135 (2025) 105023

Contents lists available at ScienceDirect

Physica Medica

journal homepage: www.elsevier.com/locate/ejmp

Original paper

Local DRL estimation and effective dose calculation in paediatric interventional cardiology using measurements and Monte Carlo simulations

Pedro Teles [a,b,*], Raquel Costa [a], Tiago Bettio [a], Teresa Pinheiro [d,e], Teresa Loupa [f], Joana Santos [g], Fátima Pinto [f], Octávia Monteiro Gil [c,e], Paolo Ferrari [h], Maria Zankl [i,1]

[a] Departamento de Física e Astronomia, Faculdade de Ciências da Universidade do Porto, rua do Campo Alegre, s/n, 4169-007 Porto, Portugal
[b] Centro de Investigação do Instituto Português de Oncologia do Porto (CI-IPOP), R. Dr. António Bernardino de Almeida s/n, 4200-072 Porto, Portugal
[c] Centro de Ciências e Tecnologias Nucleares (C2TN), Instituto Superior Técnico, Universidade de Lisboa Estrada Nacional 10 (km 139,7), 2695-066 Bobadela LRS, Portugal
[d] Instituto de Bioengenharia e Biociências, Instituto Superior Técnico, Universidade de Lisboa, Av. Rovisco Pais 1, 1049-001 Lisboa, Portugal
[e] Departamento de Engenharia e Ciências Nucleares, Instituto Superior Técnico, Universidade de Lisboa, Estrada Nacional 10 (km 139,7), 2695-066 Bobadela LRS, Portugal
[f] Centro Hospitalar de Lisboa Central – Hospital de Santa Marta, R. de Santa Marta 50, 1169-024 Lisboa, Portugal
[g] Escola Superior de Tecnologia da Saúde de Coimbra, Rua 5 de Outubro, 3046-854 Coimbra, Portugal
[h] Italian National Agency for New Technologies, Energy and Sustainable Economic Development (ENEA), Bologna, Italy
[i] Helmholtz Zentrum München, German Research Center for Environmental Health (retired), Neuherberg, Germany

ARTICLE INFO

Keywords:
Paediatric interventional cardiology
Dose reference levels (DRLs)
Monte Carlo simulations
Voxel phantoms
Effective dose estimation
Organ dose assessment
Dose conversion coefficients (DCCs)

ABSTRACT

Background: Paediatric patients with congenital heart disease benefit greatly from X-ray diagnostic and interventional procedures. However, multiple procedures lead to prolonged exposure to ionizing radiation (IR), raising concerns for secondary long-term health issues.
Purpose: This study aimed to establish local dose reference levels (LDRLs) for a National Reference Center for Congenital Cardiopathies (NRCCC) in Portugal. Additionally, it estimated effective and organ doses in paediatric patients undergoing coronary angiographies (CAs) using measurements and Monte Carlo simulations.
Methods: LDRLs were determined through statistical analysis of patient registry data from 120 patients recorded between 2022 and 2023. For effective dose estimation, personal dose equivalent values Hp(10) were measured with an anthropomorphic phantom (CIRS ATOM 705) and Raysafe dosimeters, used to validate Monte Carlo (MC) simulations, which were then employed with rescaled paediatric voxel phantoms (GsF Baby and Child), to estimate effective doses and dose conversion coefficients (DCCs) for representative patient anatomies across different age and weight groups.
Results: LDRLs for coronary angiographies at the NRCCC showed significant dose variability, indicating dose optimization opportunities. Monte Carlo simulations allowed for organ dose and effective dose calculations. Dose Conversion Coefficients were 1.107, 0.882, 0.719, and 0.524 mSv/Gy·cm^2 for newborn, 1 year-old, 5 year-old and 10 year-old groups respectively. A strong linear correlation between effective dose and air-kerma area product (KAP) was observed.
Conclusions: The study highlights the strong correlation between effective dose and KAP, offering a practical framework for estimating patient doses and enhancing radiation safety protocols in clinical practice.

1. Introduction

Congenital heart defects (CHD) affect approximately 1.35 million children annually worldwide [1]. Typically, these patients are submitted to image-guided X-ray fluoroscopy imaging to conduct catheters or needles to the lesion site to perform complex procedures in real time [2,3]. Interventional Cardiology (IC) allows specialists to avoid complicated invasive surgeries, which may be intolerable for some patients, due to their age or the pathology itself. However, the complexity of IC procedures, the long fluoroscopy times, and the potential need to

* Corresponding author.
E-mail address: ppteles@fc.up.pt (P. Teles).
[1] Retired

https://doi.org/10.1016/j.ejmp.2025.105023
Received 28 January 2025; Received in revised form 22 May 2025; Accepted 26 May 2025
Available online 11 June 2025

repeat the procedures several times lead to protracted low-dose exposure to ionizing radiation (IR). Therefore, these procedures must be optimized to minimize unnecessary risks without compromising treatment outcomes [4]. In fact, within the linear-no-threshold (LNT) model, prolonged exposure to low doses of ionizing radiation is assumed to increase the probability of stochastic effects such as radiation-induced cancers in direct proportion to the accumulated dose.

It has remained consensual, however, that despite the radiological risk, it will always be less than the clinical benefits of using IC, which saves children's lives with good quality of life outcomes [4–6]. Even if the risk factors underlying the late development of cancer remain to be fully understood [7].

The objective of this work was to perform a dosimetric analysis of paediatric patients followed at the Centro de Referência de Cardiopatias Congénitas (CR-CC, the Portuguese National Reference Center for Congenital Cardiopathies), Hospital de Santa Marta (HSM) of the Central Lisbon University Hospital CHULC) at [8].

The first step was to establish local dose reference levels (LDRLs). Establishing LDRLs is a legal requirement [9]. Existing guidelines demonstrate the importance of paediatric LDRLs, to conform to radiation protection best practices, that can lead to patient dose optimization where possible.

For this purpose, a statistical analysis of cardiac angiographies (CA) and percutaneous coronary interventions (PCI) was performed in paediatric patients for the years 2022 and 2023 to determine the Local Dose Reference Levels (LDRLs) and compare them with international guidelines.

Furthermore, Monte-Carlo simulations with anthropomorphic phantoms were used to assess organ doses as well as effective doses for patients in different age groups. This can be used to determine dose conversion coefficients and help predict organ doses/effective doses from measurable quantities such as Air-Kerma Air Product (KAP).

The Monte Carlo simulations were performed with the general code MCNP6.2 [10]. Validation of the model was made using the Raysafe i3 dosimeters [11] and the CIRS ATOM 705 (ABEL) phantom [12].

After validation, the GSF Baby and Child phantoms [13] were used to determine effective dose and organ dose due to CAs in the Antero-posterior (AP) projection at 0° from four age group representative paediatric patients (newborn, 1 year, 5 years, and 10 years).

Obtained results were analysed and compared with previously published results. Dose conversion coefficients were obtained for each age group, which can be used in clinical practice to estimate effective doses to the patients.

2. Methodology

Dosimetric quantities used in this work include the absorbed dose (mGy), in particular absorbed organ dose (also in mGy); the operational quantity personal dose equivalente Hp(10) for measurements with dosimeters (in mSv), which in the conditions of the work is equivalente to the absorbed dose in mGy: the Entrance Skin Dose (ESD) (in mGy); and finally the effective dose (mSv or relevant sub-units), determined according to the ICRP's latest reccommendations [14]. The derived quantity Air-Kerma Air Product (KAP) is provided in the convenient and more common in the literature units of cGy·cm^2, while effective Dose Conversion Coefficients (DCCs) are conveniently expressed in mSv/Gy·cm^2 (or, in the case of organ DCCs mGy/Gy·cm^2).

2.1. Dose reference Levels (DRLs)

Information from 120 patients was recorded between 2022—2023 at CR-CC of HSM/CHULC. The ages of the patients ranged between 1 day old and 19 years old. In terms of procedures, 34 % of them were diagnostic Cardiac Angiography (CA) procedures, and the remainder (63 %) were Percutaneous Coronary Interventions (PCI). From these values we determined the minimum and maximum ages, the minimum and maximum procedure lengths, as well as the mean ESD and the mean KAP, for both CA and PCI. These values are provided via the PACS system and can be found in Table 1.

Table 1 shows that mean ESDs and KAPs exhibit large standard deviations, with median values significantly smaller than the mean. This is due to their frequency distribution being highly skewed to the left and several seemingly outlier values in different ranges, as can be seen from Fig. 1, in which the histograms of the distributions of the mean ESDs and KAPs are shown for CA and PCI. The Local Dose Reference Levels for these procedures can be determined at the 75th percentile.

The European Commission's Radiation Protection n° 185 (RP 185), recommends the use of five weight groups for paediatric patients (< 5, 5-<15, 15-<30, 30-<50, and 50-<80 kg), for both for the ESD and the KAP. However, the report on DRLs for CA and PCI in the same document is provided in different weight groups (0-<10, 10-<20, etc). As such we produced the values in both weight groups. Distributions for each weight group were made for ESD (CA and PCI) and for KAP (CA and PCI). After that, the median and 75th percentile was determined, which corresponds to the LDRL for each weight group and procedure. The values obtained are shown in Tables 3 and 4, depending on the chosen weight group intervals. Also, according to RP 185, LDRLs should include at least n = 20 cases per group, which was not the case in this study. This was due to the limited number of cases referred annually to CR-CC at HSM/CHULC.

As can be seen from Table 2 the values do not strictly increase with weight group. However, they do increase with weight group in Table 3, showcasing that the RP 185 guideline is a more adequate classification.

For CA, using the more detailed 10 kg-wide weight groups, the local DRL ESD climbs steadily from 20 mGy in the 0-<10 kg group to 214 mGy in the 60-<70 kg group. A strog increase already appears at 84 mGy for 20-<30 kg, but the highest recorded CA value in this series is in the 60-<70 kg bin. The corresponding KAP rises from 156 cGy·cm^2 to 2 512 cGy·cm^2 across the same span, showing a surge at 1 078 cGy·cm^2 in 20-<30 kg. Using the broader RP 185 reccomended weight groups, CA ESD advances from 22 mGy in the < 5 kg weight group to 167 mGy for 50-<80 kg, accompanied by KAP growth from 140 cGy·cm^2 to 1 870 cGy·cm^2. The 15-<30 kg weight group shows an intermediate ESD of 88 mGy and KAP of 841 cGy·cm^2.

For PCI, both ESD and KAP are consistently higher than CA due to the complexity and duration of interventional procedures. Using the more detailed 10 kg-wide weight groups, ESD begins at 49 mGy for 0-<10 kg and peaks at 564 mGy in the 50-<60 kg group, while KAP escalates from 206 cGy·cm^2 to a maximum of 5663 cGy·cm^2 in the same 50-<60 kg group. Beyond 60 kg the available data becomes scarcer and the DRLs decrease slighlty (e.g., 84 mGy / 1 098 cGy·cm^2 for 60-<70 kg). For the RP 185 reccomended weight groups, ESD rises from 25 mGy (< 5 kg) to 49 mGy (5-<15 kg) to 312 mGy (30-<50 kg), with a modest reduction to

Table 1
Dosimetric information from PACS system of the procedures between Jan 2022 and Dec 2023 at HSM, and Local Dose Reference Level (DRL) determination.

Information	Procedure	
	Cardiac Angiography (CA)	**Percutaneous Coronary intervention (PCI)**
Minimum-maximum values patients' age	1 day old – 18 years old	28 days old – 19 years old
Minimum-maximum values Length of procedure (HH:MM:SS)	00:02:36 – 00:38:16	00:02:55 – 00:40:51
Mean ESD +/- standard deviation (mGy)	48.0 ± 53.5 mGy	99.8 ± 148.0 mGy
Median ESD (mGy)	22.0	46.0
Mean KAP +/- standard deviation (cGy·cm^2)	522.4 ± 633.5	866.5 ± 1364.7
Median KAP (cGy·cm^2)	235.0	353.0

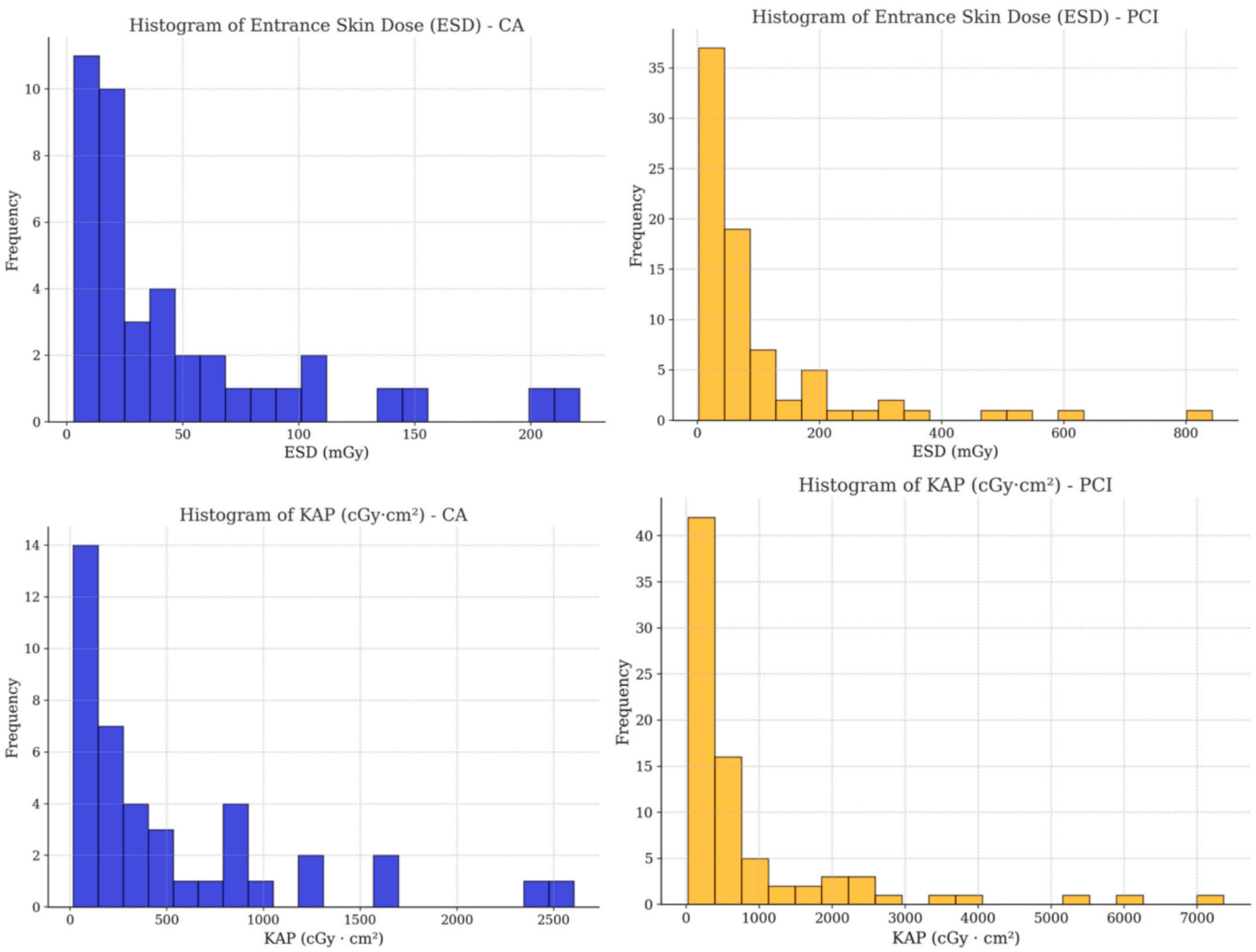

Fig. 1. Histograms of ESD and KAP for CA and PCI procedures in 2023 and 2024.

Table 2
Local Dose Reference Levels for weight groups as used for comparison with RP 185 data.

	CA			PCI		
	ESD (mGy) DLR (75th percentile)	**KAP (cGy·cm^2) DLR (75th percentile)**	**n**	**ESD (mGy) DLR (75th percentile)**	**KAP (cGy·cm^2) DLR (75th percentile)**	**n**
0-<10 kg	20	156	16	49	x	16
10-<20 kg	47	537	10	54	431	23
20-<30 kg	84	1078	3	104	894	15
30-<40 kg	–-	–-	1	179	1248	3
40-<50 kg	64	877	3	323	2191	6
50-<60 kg	140	1603	5	564	5663	8
60-<70 kg	214	2512	3	84	1098	4
70-<80 kg	–-	–-	–-	–-	–-	1
80-<90 kg	–-	–-	–-			0
90-<100 kg	–-	–-	–-	–-	–-	1
>100 kg	–-	–-	–-	202	2770	2

297 mGy in 50-<80 kg. KAP follows a similar pattern, starting at 76 cGy·cm^2 and peaking at 2398 cGy·cm^2 in the 50-<80 kg group.

For certain weight groups, due to insufficient data, DLRs are not available. In groups where there was only one value, the 75th percentile was not calculated.

The obtained LDRLs reflect the need for higher radiation exposure for larger body masses. However, this is not the only factor influencing the values, which can also change due to complexity of procedure, body mass index, or other factors.

The obtained results were compared with the results provided in RP 185, which provided data for median values of KAP for CA procedures.

Differences can be found between the results of this work and those in the literature. In Tables 4, mean KAP values are compared with data from RP 185 [16,17,18]. Caution should be taken when comparing these results, as explained in the reference [15]. Also, in Table 5, LDRLs at the 75th percentile are compared with more recent data currently available

Table 3
Local Dose Reference Levels for weight as recommended by RP 185.

	CA			PCI		
	ESD (mGy) DLR (75th percentile)	KAP (cGy·cm^2) DLR (75th percentile)	n	ESD (mGy) DLR (75th percentile)	KAP (cGy·cm^2) DLR (75th percentile)	n
< 5 kg	22	140	3	25	76	2
5-<15 kg	19	148	17	49	227	23
15-<30 kg	88	841	9	100	667	29
30-<50 kg	62	866	4	312	2067	9
50-<80 kg	167	1870	8	297	2398	13
>80 kg*	–-	–-	–-	157	2246	3

*weight group not included in the RP 5 guidelines, but added for completeness.

Table 4
Comparison of median KAP values for CA procedures obtained in this work and reported in the literature. Differences (DIF) are expressed as percentages.

Weight Group	This work (cGy • cm^2)	Harbron et al. [16] (cGy • cm^2)	% d	Barnaoui et al.[17] (cGy • cm^2)	% d	Chida et al. [18] (cGy • cm^2)	%d
<10	92	140	−34	180	−49	403	−77
10 – <20	233	220	6	260	−11	1470	−84
20 – <30	872	330	164	370	136	2540	−66
30 – <40	846	510	66	520	63	3600	−76
40 – <50	826	770	7	730	13	4670	−82
50 – <60	1279	1160	10	1030	−8	5740	−84
60 – <70	2419	1770	37	1450	66	6800	−64
70 – <80	–-	2680	–-	2050	–-	7870	–-

Table 5
Comparison of LDRLs values for CA and PCI procedures obtained in this work and the most recent reports in the literature. Differences (DIF) are expressed as percentages.

Weight group	Procedure type	This work	Giannone et al (2023) [19]	%d	Ubeda et al (2020) [20]	%d	Ubeda et al (2022) [21]	%d	Hultenmo et al (2021) [22]	%d	De Monte et al (2020) [23]	%d
< 5 kg	CA	90	80	12	430	–79	300	–70	28	221	210	–57
	PCI	72	60	21	520	–86	370	–80	32	127	220	–67
5 – < 15 kg	CA	92	120	–23	500	–82	450	–80	89	3	390	–76
	PCI	157	240	–35	800	–80	430	–63	68	131	680	–77
15 – < 30 kg	CA	576	220	162	1 260	–54	810	–29	178	224	1 540	–63
	PCI	382	230	66	1 560	–76	730	–48	185	106	940	–59
30 – < 50 kg	CA	836	540	55	4 340	–81	920	–9	575	45	1 460	–43
	PCI	875	550	59	2 550	–66	1 610	–46	914	–4	1 670	–48
50 – < 80 kg	CA	1 441	940	53	3 130	–54	2 680	–46	1 370	5	—	—
	PCI	2 137	1 130	89	3 020	–29	5 340	–60	2 325	–8	2 460	–13

[19–23],.

In general, for the low weight group patients (<10 and 10-<20) the Median KAP values obtained in this work are consistently smaller than the other presented works, which stops being the case for intermediate weight group patients (20-<30, 30-<40 and 40-<50). In any case in the case of Chida et al. the values obtained in this work are consistently smaller than those reported by this group.

The obtained LDRLs compared with more recent results in the literature [19–23], using the RP185 recommended weight groups, can be found in Table 5:

When comparing our centre's KAP DRLs with other works, it can be seen that this work's DRLs in the smallest patients (< 15 kg) are well below those reported by Ubeda and De Monte, yet are close to or slightly above the data from Giannone and Hultenmo. From 15 kg upward this work's DRLs become higher than those reported by Giannone and Hultenmo, but they still maintain much smaller values than the numbers reported by Ubeda and De Monte.

It should be noted that these results emphasize variability in dosimetric practices and the potential for optimization and perhaps harmonization of practices, which leads us to the other part of this study.

2.2. Equipment and cath lab

The CR-CC cath lab is located at the HSM/CHULC. The room has the following dimensions: 8.16 m x 7.50 m x 2.83 m, and inside it, the C-arm Innova IGS 520 [24] system is placed, as shown in Fig. 2 Further geometric details are given in the following sections.

2.2.1. Anthropomorphic paediatric phantom

An anthropomorphic phantom CIRS ATOM 705 (ABEL) was used to validate the measurements [12]. The phantom emulates a 5-year-old child, with a height of 110 cm, a weight of 19 kg, and a thorax size of 14 x 17 cm. A representation of ABEL is shown in Fig. 3:

ABEL has a sectional design, with 25 mm slices, containing anatomically correct representations of 21 internal organs. It is made of tissue-equivalent epoxy resin with 1.54 g/cm^3 density.

2.2.2. Raysafe i3 dosimeter

Raysafe i3 dosimeters provide real time personal dose equivalent rates that can be stored in a device that accompanies them. The ones used in this study were calibrated to be used in radiology settings. Green, yellow and red bars are displayed indicating the personal dose

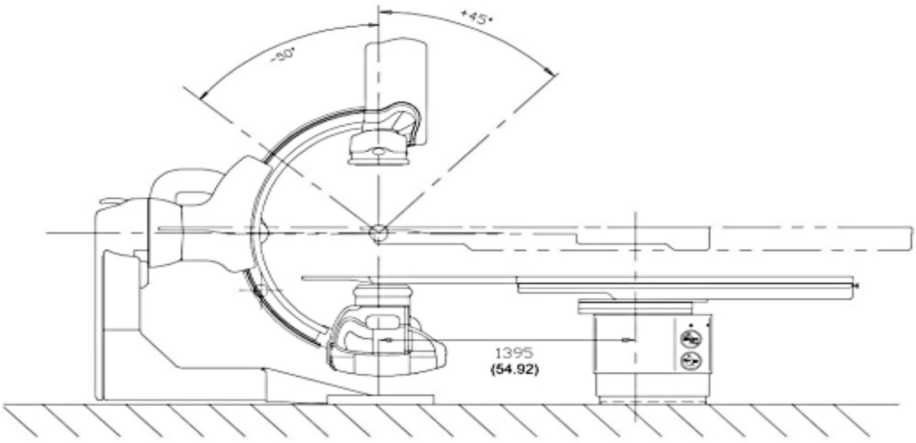

Fig. 2. Longitudinal view of the C-arm Innova IGS 520, taken from [24].

equivalent rate and the accumulated personal dose equivalent for each dosimeter [13]. Some of the main features of these dosimeters are shown in Table 6.

2.2.3. Components of the cath lab

To simulate the cath lab in a virtual environment, it was necessary to collect information about the dimensions, material compositions, and densities of the different components inside the room (Table 7). The only material for which no information could be found was that of the patient table carbon fiber, for which the stoichiometric composition, density, and internal structure were unknown.

2.3. Monte Carlo simulations

In this work, the MCNP6.2 (Monte Carlo N-Particle 6.2) code was used. MCNP6.2 is a well-known language used for particle transport [10], that uses databases of effective interaction cross-sections for 34 types of particles, such as neutrons, electrons, photons, protons, alpha particles, among others, in energy ranges from a few eV to GeV, in user-defined materials and geometries.

Photons and electrons are generated from a source according to user-specified parameters. Interaction sampling is then carried out to simulate their transport through the different user-defined geometries.

The fluence and energy deposition within each geometrical component can be followed and tallied by MCNP6.2, allowing for dosimetric calculations. For dose tallying, the *F8 tally was used, which scores the dose in MeV/particle history, for each geometric structure. Simulations were performed using $1-2\times10^{9}$ particle histories, leading to 2σ uncertainties below 2 %.

2.4. Voxel phantoms

The Helmholtz Zentrum Munchen, Baby and Child phantoms [13] were used, depictions of which are shown in Fig. 4. The main features of these phantoms are given in Table 8.

It should be noted that although the initial patients from which the images were taken to create the phantoms were from two female patients, the patients were later manually changed to possess both male and female gonads for dosimetry purposes.

3. Results and Discussion

3.1. Measurements to validate the simulation

The CIRS ATOM 705 was irradiated four times with three Raysafe dosimeters located as shown in Fig. 5.

The mean parameters taken from the DICOM file for the four irradiations are given in Table 9:

The arithmetic mean and standard deviation were taken from the obtained dose equivalent values for the four different irradiations in the three regions of interest, which are given in Table 10, together with the obtained minimum and maximum values. The gonads marked zero during the four irradiations, meaning that the equivalent dose value in this region was below the detection limit of the dosimeters. They were therefore excluded from further analysis.

Fig. 6 shows the dose distribution in the nose and heart regions. For the nose region, the standard deviation is very high, as one standard deviation below the mean value is less than the minimum dose value obtained. This is because the measured dose equivalent values are at the measurement limits of the dosimeters.

3.2. Monte Carlo simulation

The simulation environment was created using the collected data from the dosimeters and the irradiation set-up. The set-up was made by making use of the MCNP6.2 geometric tools, which consist in the definition of analytical surfaces that can be combined using Boolean operations to create “cells”, to which a given material can be ascribed. Materials (media) are created by giving the fraction by weight of each element in the compound. Values for the different materials were taken from the NIST tables [26].

3.2.1. Source and collimators

The source spectrum at 60 kVp was obtained using the IPEM78 database [25] and was placed at a source-to-surface distance (SSD) of 72 cm, equal to the measurement.

To represent the collimators, 4 copper blocks of 0.3 mm thickness were created. The upper jaws were at 20 cm distance from the source, whereas the lower jaws were 10 cm distance from it. The source-to-detector distance (SID) was defined to be at 93.8 cm as in the measurement. The aperture of the beam is 9.89°.

At the detector, the field had a 20×20 cm^2 area, with these specifications, just like in the measurements.

The X-ray tube has a total filtration of 1 mmAl equivalent; and there are two added filters, one of 0.5 mm Al and the other of 0.05 mmCu (corresponding to 1.7 mmAl at 70 keV) and finally an inherent filtration total of 2 mm Al equivalent.

In the simulation, this was simplified by considering the X-ray tube beam filtration of 1 mmAl equivalent, and then aggregating all the other filtrations in a single filtration of 2.5 mmAl (after calculations) placed next to the collimators, as shown in Fig. 7.

Fig. 7 shows the specs together with the geometric modelling of the collimators, illustrating how the upper and lower jaws are placed.

Fig. 3. Anthropomorphic phantom CIRS ATOM 705 (ABEL) [12].

Table 6
Main features of Raysafe i3 dosimeters.

Raysafe i3 dosimeters Operational Quantity	$H_p(10)$
Response time	< 1 s, above 100 μSv/h < 5 s, below 100 μSv/h
Detection limit	< 30 μSv/h
Uncertainties in dose rates (for continuous irradiation)	10 % or 10 μSv/h (40 μSv/h – 150 mSv/h) 20 % (150 mSv/h – 300 mSv/h) 40 % (300 mSv/h – 500 mSv/h)
Dose reproducibility	10 % or 1 μSv

Table 7
Geometric features of each component of the room. (a) indicate that the values have been obtained by Monte Carlo simulation analysis.

	Material	Dimensions	Density (g/cm^3)
Room	Air	8.16 m x 7.50 m x 2.83 *m*	1.2043×10^{-3}
Walls	Concrete	8.16 m x 2.83 m x 21 cm 7.50 m x 2.83 m x 21 cm	2.300
X-ray tube	Spectrum taken from IPEM 78 [25]		
Collimators	Copper	5 cm x 5 cm x 0.3 mm	8.960
Al filter	Aluminum	6 cm x 6 cm x 2.5 mm	2.699
Cu Filter	Copper	6 cm x 6 cm x 0.1 mm	8.960
Patient table	Carbon Fiber	3.35 m x (0.66 m / 0.44 m /0.20 m) x 4 cm	1.2 (a)
Patient mattress	Foam		0.085
Table base	Kevlar	48 cm x 65 cm x 94 cm	1.45
Table support	Lead	97 cm x 70 cm x 0.5 mm	11.35
Table holder	Lead	34.5 cm x 56 cm x 0.5 mm	11.35
Detector (casing)	Carbon Fiber	35 cm x 34 cm x 25 cm	1.8 (a)
Detector (glass)	Glass	31 cm x 31 cm x 1 mm	2.23
Detector	Amorphous Silicone	31 cm x 31 cm x 100 μm	2.285
C-arm	Kevlar	Semi-Circumference High: 1.83 *m* Internal Radius: 71.5 cm Thickness: 11 cm	1.45

3.2.2. ABEL simulation

The anthropomorphic phantom was created using the geometric specifications provided in the ABEL phantom specs. The phantom positioned in the centre of the table and the phantom was aligned with the source centre axis, just as in the measurements. The representation of the simulation room can be depicted in Fig. 8. The dosimeters were positioned as the real irradiation locations, heart, nose, and gonads, as can be seen in Fig. 5.

3.3. Validation and analysis

The *F8 tally was used for the calculations, which scores the deposited energy in MeV/source particle.

Results were normalised by making use of the Current intensity (mA) and the voltage (kV) of the electron beam, the mean energy value of the spectrum, the efficiency of X-ray production taken from [27], exposure time of the pulsated beam, and the attenuation of the beam through the collimators and filters.

The material and internal structure of the patient table, as well as the carbon fibre in the casing had unknown composition and density, as they appear as general carbon fibre in the manual. It was clear that both carbon fibres were different, as table carbon fibre had an internal structure, whereas the casing carbon fibre was visibly homogeneous and

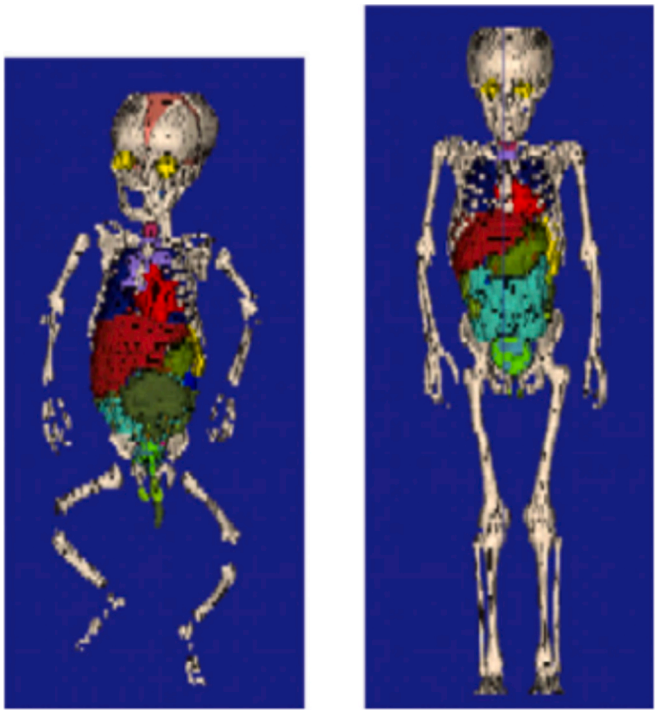

Fig. 4. Baby and Child Voxel Phantoms [13].

Table 8
Properties of the Baby and Child Voxel Phantoms.

	Baby	Child
Age	8 weeks old	7 years old
Height(cm)	57	115
Weight(kg)	4.2	21.7
Dimensions	267 × 138 × 142	256 × 256 × 144
Voxel dimensions	(0.0850 × 0.0850 × 0.4000) ≈ 0.0029 cm^3	(0.1540 × 0.1540 × 0.8000) ≈ 0.0190 cm^3

Fig. 5. CIRS ATOM 705. Dosimeter positioning: Purple dot nose, orange dot heart and black dot gonads. (For interpretation of the references to colour in this figure legend, the reader is referred to the web version of this article.)

denser. To overcome this problem, several simulations were performed using three types of fibres: PAN, OXI-PAN, and QUASI-carbon [28,29], at different densities. After comparing the simulated values with the measurements, it was observed that the simulation values giving smaller percent deviations were when considering PAN fibre of density of 1.2gcm^{-3} for the table and 1.8gcm^{-3} for the casing. This density agrees with literature values for PAN fibres with honeycomb internal structures or homogenous [29].

In this optimised set-up, the simulated dose equivalents in the nose and heart were 1.56 ± 0.04 μSv and 7.43 ± 0.17μSv, respectively. These are in accordance with the measured doses of 1.69 ± 0.39μSv and 8.35 ± 2.69μSv. The values are given in Table 11:

It should be noted that the four performed irradiations gave a broad interval of dose equivalent values for both regions, as can be seen from the standard deviations, which correspond to 32 % and 23 % for the heart and nose mean values. Compared to the percent deviations of 11 % and 7.7 %, respectively. Both values of the simulated dose equivalents have percent deviations that are smaller than one standard deviation from the mean measured dose equivalents. As such, it is safe to say that the MCNP model is statistically valid.

Table 9
Mean irradiation parameters.

Parameter	Units	Mean value
Fluoroscopy	fps	15
	kV	60
	mA	110
	Time (s)	1.097
ESD	mGy	2.5
KAP	$cGy.cm^2$	0.185
Duration	s	20
SSD	cm	72
SID	cm	93.8

Table 10
Measured mean dose equivalents, standard deviation, minima and maxima in the different regions.

Region	Mean (μSv)	Standard Deviation	Minimum (μSv)	Maximum (μSv)
Nose	1.68	0.39	1.30	2.20
Heart	8.35	2.69	5.00	12.10
Gonads	0.00	0.00	0.00	0.00

3.4. dose Calculation from the voxel phantoms

After validation, the MCNP simulation using the Baby and Child phantoms was performed. Based on data from the hospital, eight different age and weight group representative patients who underwent an anteroposterior (AP) projection (0°) CA procedure were chosen.

For the anteroposterior (AP) projection (0°) CA procedures, the used parameters corresponded to the ones in the Hospital protocols for paediatric procedures in the AP projection – 65 kV, 15.6 mA, with 10 × 10cm^2 beam size at an SID of 100 cm, and an additional Copper filtration of 0.2 mm. This additional filtration reduces dose by 32–39 % at this voltage without compromising image quality [30]. The equipment's Automatic Brightness System (ABS) varies the mA intensity for the same kV to improve image quality.

All phantoms were placed with the thorax region centred at the detector in the simulation. Using the *F8 tally, the energy received by each organ of the voxel phantoms was estimated, and from this the effective dose and the KAP were determined. Results were renormalized using the PACS measured KAP [31,32].

In Fig. 9, an illustration of a simulation using the Child phantom in AP projection is shown.

3.4.1. Voxel phantom scaling

For each patient, according to their age/weight group and anatomical features, either the Baby or the Child phantom were ascribed. After this, the dimensions of the voxel phantoms were rescaled to fit the anatomy of the patient. This rescaling was made by altering the z-dimensions of the original voxel dimensions to match the height of each patient and adjust the x and y-dimensions to match the weight, without deforming the phantoms [33–37]. The obtained values, together with the most important features of the procedures, are shown in Table 12.

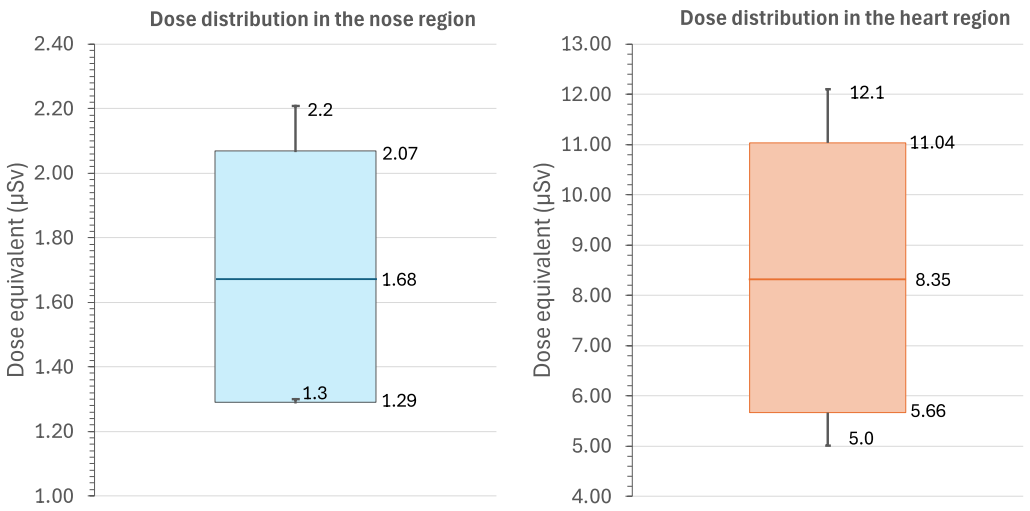

Fig. 6. Dose equivalent in the nose and heart regions.

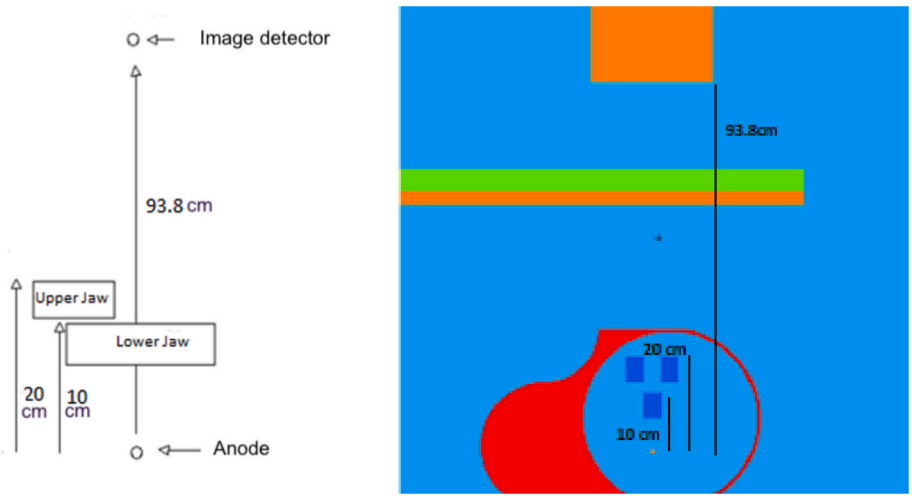

Fig. 7. Left: representation of the upper and lower jaws in the equipment's blueprints. Right: Geometric representation of the collimators in the simulation.

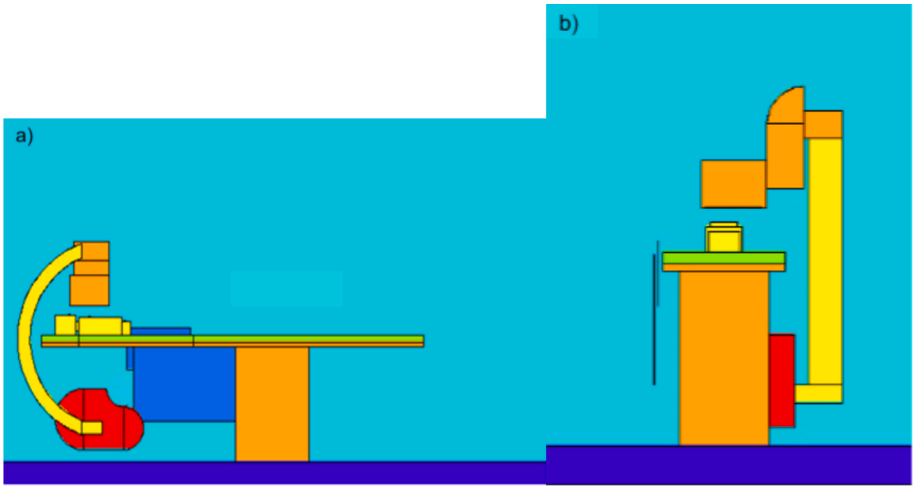

Fig. 8. Simulated room and equipment with the ABEL phantom in (a) longitudinal view (b) cross-sectional view.

3.4.2. Absorbed organ doses and effective doses

Organ doses in the bone and bone marrow were calculated using data from [38]. Results were obtained for each organ, and the effective dose determined by applying the tissue weighting factors to each region and then summing the results. As the gender of the patients was known the gonads value varied according to gender.

Table 11
Simulated dose equivalents measured mean dose equivalents and corresponding standard deviations. The relative difference is expressed as a percentage.

Region	Simulated dose equivalent ± sd (**μSv**)	Measured dose equivalent mean ± sd (**μSv**)	Relative difference (%)
Heart	7.43 ± 0.17	8.35 ± 2.69(32%)	11.0 %
Nose	1.56 ± 0.04	1.69 ± 0.39(23 %)	7.7 %

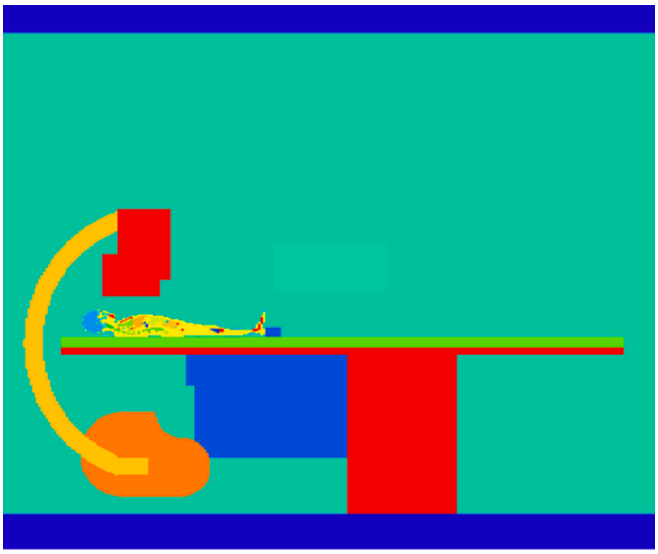

Fig. 9. Illustration of a simulation using the Child phantom in the AP projection.

In Table 13, values for the effective dose, as well as PACS provided KAP and Entrance Skin Doses (ESD) are provided, together with the calculated dose conversion coefficients (DCC) for each patient/age group.

Effective dose values (mSv) are within the range interval of values published by [39,40]. It should be noted, however, that previously reported KAP values seem to vary significantly in the literature [40,41]. Obtained dose conversion factors of 1.107 mSv/Gy • cm^2, 0.882 mSv/Gy • cm^2, 0.719 mSv/Gy • cm^2 and 0.524 mSv/Gy • cm^2 for the newborn, 1–5, 5–10 and 10–15-year-old age groups also agree with previous published results [39].

For adult patients, it is common to assume that there is a linear correlation between the effective dose and measured KAP (cGy • cm^2) [43], although for children it would be wise to do this in different age or weight groups, this is impossible considering the size of our study. However, a very adequate fit is obtained for the effective dose (E) as a function of KAP ($R^2 = 0.9724$), with a slope of 7.308 mSv/Gy • cm^2, as shown in Fig. 10.

This linear correlation seems to indicate that the curve could be used to predict effective doses for this equipment and procedures from KAP. This could have clinical relevance, although more data should be obtained.

3.5. Organ doses

In Table 14, the obtained absorbed dose to selected organs is shown.

The obtained organ dose values are within range of previously published results [38,42]. Fig. 11 shows a plot of the variation of organ dose with KAP.

The obtained values show that for practically all organs (except the bladder), the least and highest values correspond to the least and highest values of the used KAP. For instance, in the heart and lungs, values vary between 0.43 mGy for the heart and 2.04 mGy for the lung, in the case of the 2 year old with a KAP of 88 cGy • cm^2; and 2.04 mGy for the heart and 7.67 mGy for the lung in the case of the 5 year old with a KAP of 702 cGy • cm^2, corresponding to the least and highest used KAP. Estimated values for the red bone marrow vary between 0.50 mGy for the 88 cGy • cm^2, and 4.50 mGy for the 702 cGy • cm^2.

Linear fits were made to the organ doses as a function of KAP. The obtained fits varied between having a goodness-of-fit measured as R^2 from a negative value for the bladder (meaning no linear correlation) to values closer to 1 for the lungs ($R^2 = 0.941$), spinal cord ($R^2 = 0.912$), and bone marrow ($R^2 = 0.897$), for instance. In Table 13, the KAP-to-organ dose coefficients are given as obtained with the linear fits, for R^2 values higher than 0.75:

An $R^2 > 0.75$ means that over 75 % of the variation in the dependent variable (organ dose) can be explained by the independent variable (KAP), as such organ dose can be fairly well estimated using the coefficients in Table 15 This can also help clinicians in determining, not only a cumulated effective dose, but also cumulated organ doses, albeit with higher uncertainties [44].

Table 12
Patients and PACS data and respective rescaled phantom to match their anatomy.

Procedure	1	2	3	4	5	6	7	8
Age	5 days old	2 months old	11 months old	2 years old	4 years old	5 years old	5 years old	11 years old
Age group	newborn	newborn	1–5 yo	1–5 yo	5–10 yo	5–10 yo	5–10 yo	10–15 yo
Height (cm)	51	51	77	79	100	107	98	140
Weight (kg)	4.3	5.0	6.4	10	15	16	18	23
Weight group (kg)	< 5	5-<15	5-<15	5-<15	15-<30	15-<30	15-<30	15-<30
Duration (hh:mm:ss)	00:33:48	00:12:10	00:25:42	00:09:06	00:08:05	00:33:35	00:36:31	00:10:58
Total dose (mSv)	40	44	101	12	21	39	103	22
KAP ($cGy.cm^2$)	190	157	454	88	235	568	702	382
Gender	M	M	F	M	M	F	F	M
Phantom	Baby	Baby	Baby	Baby	Child	Child	Child	Child
Matrix dimensions	267 × 138 × 142	267 × 138 × 142	267 × 138 × 142	267 × 138 × 142	256 × 256 × 144	256 × 256 × 144	256 × 256 × 144	256 × 256 × 144
Voxel dimensions (cm^3)	0.0952 × 0.0952 × 0.3592 ≈ 0.0033	0.103 × 0.103 × 0.3592 ≈ 0.0038	0.095 × 0.095 × 0.5425 ≈ 0.0049	0.117 × 0.117 × 0.556 ≈ 0.0076	0.128 × 0.128 × 0.704 ≈ 0.0114	0.135 × 0.135 × 0.743 ≈ 0.014	0.150 × 0.150 × 0.681	0.142 × 0.142 × 0.979 ≈ 0.020
Physical dimensions (cm^3)	25.42 X 13.14 X 51.0	27.54 × 14.2 × 51.0	25.3 × 13.1 × 77.0	31.2 × 16.2 × 79.0	34.0 × 17.6 × 100.0	34.6 × 34.6 × 107	38.4 × 38.4 × 98.0	36.4 × 36.4 × 141

Table 13
Obtained total effective doses (mSv) for the different patients, divided into age groups, together with KAP (cGy • cm^2), and DCC (mSv/Gy • cm^2).

Patient	Age	Age Group	Weight (kg)	Equipment KAP (cGy.cm^2)	Equipment ESD (mGy)	Estimated Effective Dose [**mSv**]	U (%)	DCC (**mSv/Gy.cm^2**)	Mean DCC
1	5 do	Newborn	4.3	190	40	2.17	2.13	1.382	1.107
2	2 mo		5.0	157	44	1.87	2.11	1.191	
3	11 mo		6.4	454	101	3.39	2.89	0.747	
4	2 yo	1 – 5 years old	10	88	12	0.75	2.68	0.860	0.882
5	4 yo		15	235	21	2.12	2.86	0.903	
6	5 yo	5–10 years old	16	568	39	4.08	1.36	0.718	0.719
7	5 yo		18	702	93	5.05	1.20	0.719	
8	11 yo	10–15 years old	23	382	22	2.00	1.44	0.524	0.524

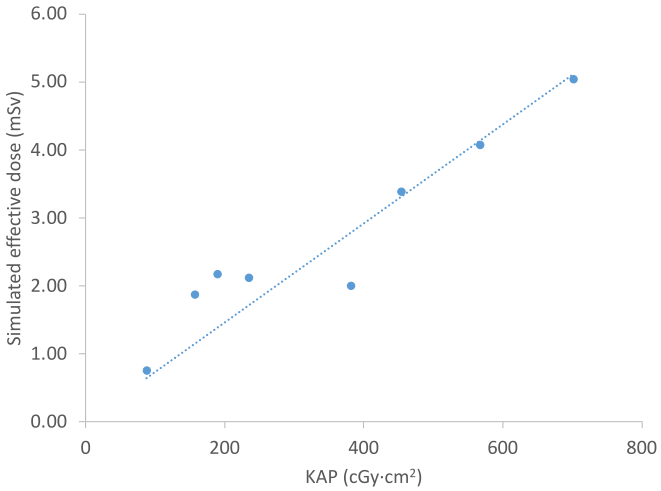

Fig. 10. Effective dose as a function of KAP.

3.6. Uncertainty analysis

The uncertainty in the calculations should consider a combination of the contributions to the uncertainty from the Monte Carlo simulations, the measurements, the uncertainties with the materials and the phantom rescaling.

While statistical uncertainties from Monte Carlo simulations were < 3 %, the optimization of the unknown densities and compositions of materials introduced a high uncertainty of 7.7–11 % (corresponding to the standard deviation of the values we obtained), validated against measured values. Finally, assuming an estimated 3 % to the phantom rescaling to align voxel phantoms with patient-specific anatomy, these contributions, using the root-sum-square method, provide a total uncertainty in the effective dose values of approximately 10 %. This level of uncertainty aligns with published paediatric dosimetry studies.

4. Conclusions

The present work aimed to evaluate the radiation doses received in the organs of paediatric patients with congenital heart disease during diagnostic and interventional cardiology procedures using Monte Carlo simulations and voxel phantoms.

The importance of this work and their future integration into clinical practice in a paediatric reference hospital is related to the need to estimate the cumulated doses these patients receive throughout their lives and consider measures to mitigate them. This could help in dose optimization and raising awareness of staff and help in the implementation of a dose monitoring programme [45].

A statistical analysis of the paediatric patients allowed for the determination of local dose reference levels for the reference centre CR-CC at HSM/CHULC, which were, when using the 10-by-10 kg intervals, for CA: 156 cGy·cm^2 for the 0–<10 kg weight group, 537 cGy·cm^2 for the 10–<20 kg weight group, 1078 cGy·cm^2 for the 20–<30 kg weight group, 877 cGy·cm^2 for the 40–<50 kg weight group, 1603 cGy·cm^2 for the 50–<60 kg weight group and 2512 cGy·cm^2 for the 60–<70 kg weight group. For PCI, the values were: 206 cGy·cm^2, 431 cGy·cm^2, 894

Table 14
Selected organ doses for the different patients.

Age	**5 days old**		**2 months old**		**11 months old**		**2 years old**		**4 years old**		**5 year old**		**5 year old II**		**11 year old**	
weight (kg)	**4.3**		**5.0**		**6.4**		**10**		**15**		**16**		**18**		**23**	
KAP(cGy.cm^2)	**190**		**157**		**454**		**88**		**235**		**568**		**702**		**382**	
Organ	**organ dose (mGy)**	**u**	**organ dose (mGy)**	**u**	**organ dose (mGy)**	**u**	**organ dose (mGy)**	**u**	**organ dose (mGy)**	**u**	**organ dose (mGy)**	**u**	**organ dose (mGy)**	**u**	**organ dose (mGy)**	**u**
Heart	0.69	0.00	0.59	0.00	1.85	0.00	0.43	0.00	1.49	0.00	2.00	0.00	2.04	0.00	1.27	0.00
Lungs	1.96	0.01	1.70	0.01	5.01	0.01	1.20	0.00	4.09	0.01	6.95	0.02	7.67	0.02	4.62	0.01
Stomach	0.67	0.01	0.55	0.01	1.29	0.01	0.30	0.00	0.74	0.01	1.24	0.01	1.08	0.01	0.65	0.00
Colon	0.46	0.01	0.38	0.01	0.45	0.00	0.11	0.00	0.24	0.00	0.69	0.01	0.70	0.02	0.30	0.01
Red bone marrow	1,62	0.20	1.46	0.20	2.28	0.19	0.50	0.16	1.20	0.17	2.84	0.16	4.16	0.04	2.04	0.24
Gonads	0.03	0.00	0.03	0.00	2.24	0.16	0.01	0.00	0.02	0.00	3.20	0.11	3.31	0.12	0.01	0.00
Bladder	0.17	0.00	0.14	0.00	0.15	0.00	0.04	0.00	0.07	0.00	0.10	0.00	0.12	0.00	0.03	0.00
Liver	0.46	0.00	0.38	0.00	0.85	0.00	0.21	0.00	0.63	0.00	1.22	0.00	1.08	0.00	0.79	0.00
Thyroid	0.53	0.01	0.48	0.01	1.29	0.01	0.29	0.00	0.63	0.00	1.42	0.01	2.60	0.02	0.58	0.00
Brain	0.10	0.00	0.10	0.00	0.10	0.00	0.02	0.00	0.04	0.00	0.12	0.00	0.26	0.00	0.04	0.00
Kidneys	0.99	0.01	0.81	0.01	0.92	0.02	0.26	0.00	0.62	0.01	1.60	0.01	1.48	0.01	0.73	0.00
Spinal cord	0.75	0.00	0.67	0.00	1.41	0.00	0.40	0.00	1.26	0.01	2.01	0.00	2.38	0.00	1.19	0.00
Spleen	0.51	0.00	0.43	0.00	0.98	0.01	0.24	0.00	0.68	0.00	1.54	0.00	1.30	0.00	0.77	0.00
Eye lenses	0.07	0.01	0.06	0.00	0.06	0.01	0.01	0.00	0.03	0.00	0.07	0.01	0.11	0.01	0.03	0.00

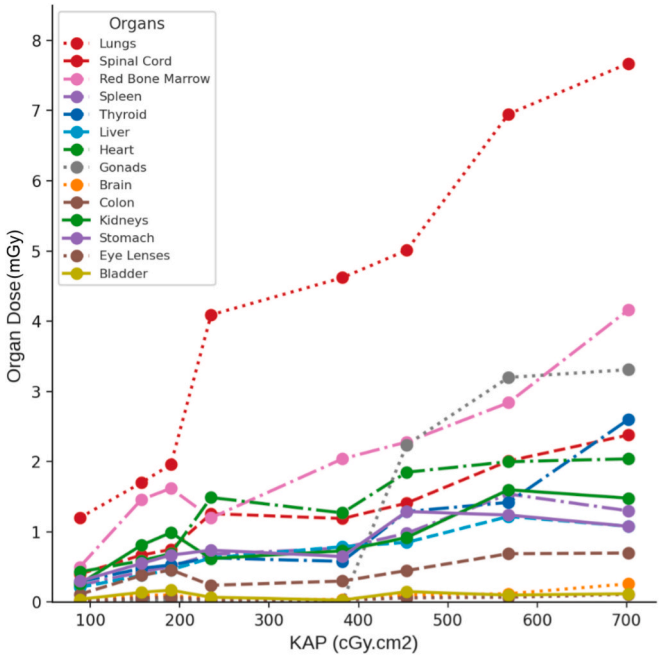

Fig. 11. Selected organ doses vs KAP (cGy • cm^2).

Table 15
Organ dose to KAP conversion coefficient from the linear fits.

Organ	conversion coefficient (*mGy*/Gy • cm^2)	R^2
Lungs	1.168	0.941
Red Bone Marrow	0.559	0.897
Heart	0.349	0.764
Spinal Cord	0.347	0.912
Thyroid	0.293	0.842
Spleen	0.222	0.860
Liver	0.190	0.835

cGy·cm^2, 1 248 cGy·cm^2, 2 191 cGy·cm^2, 5 663 cGy·cm^2 and 2 345 cGy·cm^2 for the same respective weight groups.

When applying the recommended RP 185 wt groups, for CA the LDRLS were: 140 cGy·cm^2 for the < 5 kg group, 148 cGy·cm^2 for the 5–< 15 kg group, 841 cGy·cm^2 for the 15–< 30 kg group, 867 cGy·cm^2 for the 30–< 50 kg group, and 1870 cGy·cm^2 for the 50–< 80 kg group. For PCI these values were 76 cGy·cm^2, 227 cGy·cm^2, 667 cGy·cm^2, 2067 cGy·cm^2 and 2398 cGy·cm^2 for the same respective weight groups.

Comparison with the more recent LDRLs published in the literature shows that, in the lower weight groups, the CR-CC at HSM/CHULC's LDRLs are well optimized relative to other reported values. However. there is room for optimization in patients with weights above the 15-<30 kg weight group, in particular for PCI.

The patient cohort at n = 120 does not fully comply with RP 185′s guideline of a minimum of n = 20 values for each group. Nevertheless, the results obtained still hold local clinical reference and serve as a possible starting point for more future studies to be performed.

A more detailed dosimetric analysis was performed using Monte Carlo simulations, measurements with anthropomorphic phantom ABEL (CRIS ATOM 705) and dosimeters. This allowed the estimation of organ doses and effective dose in real patient scenarios in an AP projection CA procedure.

The validation of the Monte Carlo model was made by comparing the simulations with measurements. This led to simulated doses in the nose and the heart of 1.56 ± 0.04μSv and 7.43 ± 0.17μSv, respectively within one standard deviation of the mean values obtained with the measurements.

The optimized model was used to simulate eight real AP projection CA procedures, using rescaled voxel phantoms to simulate the patients. The simulated procedures corresponded to interventional procedures in patients aged 5 days, 2 months, 11 months, 2 years, 4, years, 5 years (two), and 11 years old, representative of different age and weight groups and varying KAP values between 88 and 702 cGy·cm^2. The GSF Baby and Child voxel phantoms were rescaled to have the same weight, and height as the patients in question, without deforming the phantoms. Equivalent doses were calculated for all organs.

The calculated effective doses were 2.17 mSv with a KAP of 190 cGy·cm^2 (DCC = 13.820 μSv/cGy·cm^2); 1.87 mSv with a KAP of 157 cGy·cm^2 (DCC = 11.910 μSv/cGy·cm^2); 3.39 mSv with a KAP of 454 cGy·cm^2 (DCC = 7.470 μSv/cGy·cm^2); 0.75 mSv with a KAP of 88 cGy·cm^2 (DCC = 8.600 μSv/cGy·cm^2); 2.12 mSv with a KAP of 235 cGy·cm^2 (DCC = 9.030 μSv/cGy·cm^2); 4.08 with a KAP of 568 cGy·cm^2 (DCC = 7.180 μSv/cGy·cm^2); 5.05 mSv with a KAP of 702 cGy·cm^2 (DCC = 7.190 μSv/cGy·cm^2), and 2.00 mSv with a KAP of 382 cGy·cm^2 (DCC = 5.240 μSv/cGy·cm^2), for the 5-day-old, 2 month-old, 11-month-old, 4-year-old, 5-year-old (1), 5-year-old(2), and 11-year-old, respectively.

The obtained values for effective dose were shown to have a linear correlation with the used KAP values, with a goodness-of-fit of $R^2 = 0.9724$ and a slope of 7.308 μSv/cGy • cm^2. This demonstrates the clinical applicability of this model, which can be used to determine effective dose for a patient, knowing the KAP. Similar linear fits were performed for organ doses alone, yielding worse goodness-of-fits but still reliable, which can be used to determine organ doses from KAP. Future work should involve the simulation of more patients to verify this linearity and divide it in age and weight groups if possible. Also, simulations should be performed in the weight groups 30-<50 kg and > 50 kg which were not envisaged in this study.

Additionally, the developed model opens the possibility of studying other procedures of various complexities, enabling the acquisition of dose information in different organs of paediatric patients.

Finally, this work demonstrated the importance and need to implement methods for evaluating cumulated doses in paediatric patients with congenital heart disease. The developed methodology will allow for the transfer to clinical practice of processes for dose control and mitigation, contributing to improving radiological protection practices in interventional cardiology.

Declaration of competing interest

The authors declare that they have no known competing financial interests or personal relationships that could have appeared to influence the work reported in this paper.

References

[1] Image Gently, "Have-A-Heart and Image Gently." https://www.imagegently.org/Procedures/Cardiac-Imaging (accessed Jun 12, 2024).
[2] Costa R. Estudo dosimétrico da exposição de pacientes pediátricos com cardiopatias congénitas a raios-X devido a procedimentos de cardiologia de intervenção. Thesis: MSc; 2022. https://hdl.handle.net/10216/148817 (accessed Jun 12, 2024.
[3] Baim D. Cardiac Catheterization, Angiography, and Intervention. Boston 2001.
[4] Vañó E, Arranz L, Sastre JM, Moro J, Ledo J, Garate P, et al. Dosimetric and radiation protection considerations based on some cases of patient skin injuries in interventional cardiology. Br J Radiol 1998;71:510–6. https://doi.org/10.1259/bjr.71.845.9691896.
[5] C. Karazisi, E. Dellborg, H. Johansson Boman, M. Holm, P. Lidenmark, Risk of cancer in young and older patients with congenital heart disease and the excess risk of cancer by syndromes, organ transplantation and cardiac surgery: Swedish health registry study (1930–2017), Lancet Reg. Heal. - Eur. 18 (2022). https://doi.org/10.1016/J.LANEPE.2022.100407.
[6] Cohen S, Gurvitz MZ, Beauséjour-Ladouceur V, Lawler PR, Therrien J, Marelli AJ. Cancer Risk in Congenital Heart Disease-What Is the Evidence? Can J Cardiol 2019;35:1750–61. https://doi.org/10.1016/J.CJCA.2019.09.023.
[7] Campolo J, Annoni G, Giaccardi M, Andreassi MG. Congenital Heart Disease and the Risk of Cancer: An Update on the Genetic Etiology, Radiation Exposure Damage, and Future Research Strategies. J Cardiovasc Dev Dis 2022;9:245. https://doi.org/10.3390/JCDD9080245.

[8] Hospital de Santa Marta, url: https://www.chlc.min-saude.pt/hospital-santa-marta/ (in Portuguese), last visited: 03/12/2024.

[9] Decreto-lei (Decree-law) 108/2018 which transposes the EU Directive 2013/59/EURATOM (url: https://diariodarepublica.pt/dr/detalhe/decreto-lei/108-2018-117202785), last visited: 03/12/2024.

[10] Los Alamos National Laboratory, MCNP6.2 User's Manual. LA-CP-14-00745 (2014).

[11] Fluke Corporation, "RaySafe i3," 2017. Accessed: Jun 12, 2024. [Online]. Available: https://www.raysafe.com/sites/default/files/2019-01/5200121-1.3_RaySafe_i3_PDM2_leaflet_EN_web.pdf.

[12] ATOM, "Dosimetry Verification Phantoms," USA, 2013. Accessed: Oct. 10, 2021. [Online]. Available: https://www.cirsinc.com/wp-content/uploads/2020/08/701-706-DS-082020-1.pdf.

[13] Petoussi-Henss N, Zankl M, Fill U, Regulla D. The GSF family of voxel phantoms. Phys Med Biol 2002;47(1):89. https://doi.org/10.1088/0031-9155/47/1/307.

[14] International Commission on Radiological Protection. (2007). The 2007 Recommendations of the International Commission on Radiological Protection. Annals of the ICRP, 37(2–4). ICRP Publication 103.

[15] European Commission. *European Guidelines on Diagnostic Reference Levels for Paediatric Imaging. Radiation Protection No. 185*, European Commission, Brussels, 2010.

[16] Harbron RW, Pearce MS, Salotti JA, McHugh K, McLaren C, Abernethy L, et al. Radiation doses from fluoroscopically guided cardiac catheterization procedures in children and young adults in the United Kingdom: a multicentre study. Br J Radiol 2014;88(1050):20140282. https://doi.org/10.1259/bjr.20140282.

[17] Barnaoui S, Rehel JL, Baysson H, Boudjemline Y, Girodon B, Bernier MO, et al. Local reference levels and organ doses from paediatric cardiac interventional procedures. Pediatr Cardiol 2014;35(6):1037–45. https://doi.org/10.1007/s00246-014-0895-5.

[18] Chida K, Ohno T, Kakizaki S, Takegawa M, Yuuki H, Nakada M, et al. Radiation dose to the paediatric cardiac catheterization and intervention patient. AJR Am J Roentgenol 2010;195(5):1175–9. https://doi.org/10.2214/AJR.10.4466.

[19] Giannone A, De Monte F, Colangelo M, Di Salvo G, Fraccaro C, Sirico D, et al. Standardized diagnostic reference levels for paediatric interventional cardiology: Data from an Italian referral centre. *Phys Med* 2024;124:104487. https://doi.org/10.1016/j.ejmp.2024.104487.

[20] Ubeda C, Carrasco P, Muñoz E, Miranda P, Otalora R, Vano E. Patient radiation doses in paediatric interventional cardiology and optimisation actions. *Radiat Phys Chem* 2020;168:108539. https://doi.org/10.1016/j.radphyschem.2019.108539.

[21] Ubeda C, Vañó E, Sánchez R, Rincón F, Carrasco P, Muñoz E, et al. Setting up regional diagnostic reference levels for paediatric interventional cardiology in Latin America and the Caribbean countries: Preliminary results and identified challenges. *J Radiol Prot* 2022;42(3):040501. https://doi.org/10.1088/1361-6498/ac87b7.

[22] Hultenmo M, Nygren A, Söderberg B, Wåhlander H. Dose evaluation and proposal of local diagnostic reference levels for paediatric cardiac catheterizations performed on a high-sensitivity angiographic system allowing low-dose imaging. *Radiat Prot Dosim* 2021;195(3–4):279–88. https://doi.org/10.1093/rpd/ncab072.

[23] De Monte F, Giannone A, Paiusco M, Castaldi B. Typical values for paediatric interventional cardiology catheterisations: A standardised approach towards diagnostic reference level establishment. *Phys Med* 2020;76:134–41. https://doi.org/10.1016/j.ejmp.2020.07.001.

[24] General Electric Healthcare, "Innova IGS 5 with AutoRight." https://www.gehealthcare.com/products/image-guiding-solutions/innova-igs-520 (accessed Jun 12, 2024).

[25] G.D. Morrison, Catalogue of Diagnostic X-ray Spectra and Other Data (IPEM Report 78), K. Cranley, B.J. Gilmore, G.W.A. Fogarty, L. Desponds (Eds.), The Institution of Physics and Engineering in Medicine and Biology (1997). Radiography. 4 (1998) 228-9.

[26] NIST, "X-Ray Mass Attenuation Coefficients" NIST Standard Reference Database 126. https://physics.nist.gov/PhysRefData/XrayMassCoef/tab1.html (accessed Jun 12, 2024).

[27] P. Sprawls, "X-Ray Production," the physical principles of medical imaging, 201, 2014. http://www.sprawls.org/ (accessed Jun 12, 2024).

[28] Cho D, Choi Y, Park JK, Lee J, Yoon BI, Lim YS. Thermal Conductivity and Thermal Expansion Behavior of Pseudo-Unidirectional and 2-Directional Quasi-Carbon Fiber/Phenolic Composites. Fibers Polym 2004;5:31–8.

[29] Gulgunje PV, Newcomb BA, Gupta K, Chae HG, Tsotsis TK, Kumar S. Low-density and high-modulus carbon fibers from polyacrylonitrile with honeycomb structure. Carbon 2015;95:710–4. https://doi.org/10.1016/j.carbon.2015.08.097.

[30] Brosi P, Stuessi A, Verdun FR, Vock P, Wolf R. Copper filtration in paediatric digital X-ray imaging: its impact on image quality and dose. *Radiol Phys Technol* 2011;4(2):148–55. https://doi.org/10.1007/s12194-011-0115-4.

[31] Ferrari P, Jovanovic Z, Bakhanova E, Becker F, Krstic D, Jansen J, et al. Absorbed dose in the operator's brain in interventional radiology practices: evaluation through KAP value conversion factors. *Phys Med* 2020. https://doi.org/10.1016/j.ejmp.2020.07.011.

[32] Ferrari P, Becker F, Campani L, Jansen J, Jovanović Z, Krstić D, et al. On the placement of apron dosemeters and dose assessment in interventional cardiology procedures: Preliminary results. *Radiat Prot Dosim* 2022;198(19):1495–9. https://doi.org/10.1093/rpd/ncac188.

[33] Christy M, Eckerman KF. Specific absorbed fractions of energy at various ages from internal photon sources. Oak Ridge, TN: Oak Ridge National. Laboratory 1987. https://doi.org/10.2172/5737969.

[34] Teles P, Mendes M, Zankl M, de Sousa V, Santos AI, Vaz P. Assessment of the absorbed dose in the kidney of nuclear nephrology paediatric patients using ICRP biokinetic data and Monte Carlo simulations with mass-scaled paediatric voxel models. *Radiat Prot Dosim* 2017;174(1):121–35.

[35] Zankl M, Becker J, Schlattl H, Petoussi-Henss N, Regulla D. Computational phantoms of the ICRP reference male and reference female. Radiation Protection Dosimetry. 131(1), 115–120.

[36] Stabin MG, Xu XG, Emmons MA, Segars WP, Shi C, Fernald MJ. RADAR Reference Adult, Pediatric, and Pregnant Female Phantom Series for Internal and External Dosimetry. Journal of Nuclear Medicine 53(11), 1807–1813. doi:10.2967/jnumed.112.106138.

[37] Stepusin EJ, Long DJ, Marshall EL, Bolch WE. Assessment of different patient-to-phantom matching criteria applied in Monte Carlo–based computed tomography dosimetry. Medical Physics 44(10), 5498–5508. doi:10.1002/mp.12502.

[38] Cristy M. Active bone marrow distribution as a function of age in humans. *Phys Med Biol* 1981;26(3):389–400.

[39] Sarycheva SS. Effective dose in paediatric interventional cardiology. *Radiat Prot Dosim* 2021;195(3–4):273–8. https://doi.org/10.1093/rpd/ncab053.

[40] Varghese A, Devi A, George PV, Livingstone RS. Radiation dose and risk in children undergoing cardiac interventions performed using flat detector angiography systems. *J Radiol Prot* 2017;37(4).

[41] Abuzaid M, Abdelrazig A, Sulieman A, Alkhorayef M, Babikir E, Alonazi B, et al. Radiation dose to the paediatric undergoing diagnostic coronary angiography and percutaneous intervention procedures. *Radiat Phys Chem* 2020;167:108265. https://doi.org/10.1016/j.radphyschem.2019.04.015.

[42] Rizk C, Fares G, Vanhavere F, Saliba Z, Farah J. Diagnostic reference levels, deterministic and stochastic risks in paediatric interventional cardiology procedures. *Health Phys* 2020;118(1):85–95. https://doi.org/10.1097/HP.0000000000001114.

[43] Compagnone G, Ortolani P, Domenichelli S, Ovi V, Califano G, Dall'Ara, G., & Marzocchi, A.. Effective and equivalent organ doses in patients undergoing coronary angiography and percutaneous coronary interventions. *Med Phys* 2011;38(4):2168. https://doi.org/10.1118/1.3561508.

[44] Karambatsakidou A, Omar A, Fransson A, Poludniowski G. Calculating organ and effective doses in paediatric interventional cardiac radiology based on DICOM structured reports – Is detailed examination data critical to dose estimates? *Phys Med* 2019;57:17–24.

[45] Hill KD, Frush DP, Han BK, Abbott BG, Armstrong AK, DeKemp RA, et al. Radiation safety in children with congenital and acquired heart disease: A scientific position statement on multimodality dose optimization from the Image Gently Alliance. *J Am Coll Cardiol Img* 2017;10(7):797–818. https://doi.org/10.1016/j.jcmg.2017.04.003.